Hindawi
Mathematical Problems in Engineering
Volume 2020, Article ID 9768904, 12 pages
https://doi.org/10.1155/2020/9768904

Research Article

Modeling of Coupling Mechanism between Ballast Bed and Track Structure of High-Speed Railway

Xuejun Wang, Jianghua Pu, Peng Wu, and Mingfang Chen

Faculty of Mechanical and Electrical Engineering, Kunming University of Science and Technology, Kunming 650500, China

Correspondence should be addressed to Mingfang Chen; mfchen111@sina.com

Received 18 December 2019; Accepted 20 January 2020; Published 21 February 2020

Guest Editor: Weicun Zhang

In this paper, a discrete and continuous body coupling algorithm is used to study the dynamic contact characteristics between ballasts and between ballasts and track structures. Firstly, the three-dimensional fine modeling of ballast particles is realized based on the three-dimensional laser scanning method, and then through the discrete and continuum coupling algorithm from the micro-macro point of view, a multiscale and unified particle-track structure coupling model is established. Based on the coupling model, the macro- and microdynamic characteristics of the ballast bed and the mechanical characteristics of the track structure under the dynamic load of high-speed trains with different driving speeds are studied. It is shown that the cumulative settlement of the ballast bed is directly proportional to the contact force and rotation speed of the ballast, and the faster the driving speed is, the greater the cumulative deposition speed and cumulative settlement of the ballast are. The contact force between the ballast and sleeper mainly comes from the bottom of the sleeper, and its contact force and contact strength increase with the increase of driving speed.

1. Introduction

Ballasted track is an important part of the track structure of high-speed railway, which has the advantages of good elasticity, easy maintenance, and fine noise absorption. As a key part of the ballast track structure, the ballast bed is mainly composed of crushed stone ballast, which directly suffers the train load transmitted by sleepers. With the increase of train speed, the train load and frequency of track structure expand, which accelerates the accumulated deformation and uneven settlement of the ballast bed [1]. The deterioration of the ballasted track bed increases the track irregularity and enhances the wheel rail power. The vicious cycle formed by the two will directly affect the service status of the track structure and the safety and ride comfort of train operation. Therefore, many studies have been carried out on the interaction between the ballast bed and track structure.

In terms of experimental research, Kaynia et al. [2] studied the test results of ground and subgrade vibration response when high-speed trains pass on the southern line of Sweden and proposed the evaluation model of ground and subgrade vibration at different positions. Shaer et al. [3] built a 1 : 3 scale track model to study the deformation and settlement characteristics of the ballasted track under repeated load and pointed out the correlation between track settlement and sleeper vibration acceleration. Ishikawa et al. [4] studied the distribution characteristics of internal stress of subgrade and the development law of track settlement under changeful load through an 1 : 5 indoor model test of the ballasted track. Koike et al. [5] used the 1 : 5 shrinking test model to test the lateral resistance of six different types of sleepers. Kennedy [6] established a full-scale test model system (GRAFT) for ballasted track and subgrade, studied the influence of subgrade deformation modulus on the subsidence of the ballasted track, and proposed a prediction method for the subsidence of the ballasted track with load amplitude, subgrade deformation modulus, and other factors. Jing et al. [7] carried out field tests to compare and analyze the lateral resistance of type III sleepers under different geometric sections of the ballast bed and the lateral resistance of ladder sleepers under different ballast shoulder widths of the ballast bed. In addition to the track model, the

loading system is also important for the test. Among them, Faghihi Kashani et al. [8], Momoya et al. [9], and Yu et al. [10] use the actuator controlled by hydraulic servocontrol system to load. The hydraulic servosystem is a nonlinear system; in order to achieve the accuracy and stability of dynamic wheel load simulation, it is necessary to adopt efficient control methods. As a new control method, U-model is an effective method for the nonlinear control system design [11]. For U-model research, by Zhu et al. [12], the first and second feedback adaptive control platforms of the nonlinear system are established based on U-model. At the same time, a U-neural network (U-NN) structure is proposed to facilitate the design and control of all dynamic systems modeled by linear/nonlinear polynomials/state space equations [13]. In addition, Geng et al. [14] proposed a predictive control scheme based on U-model, which solves the problem of input delay in nonlinear systems.

As it is difficult to analyze the microcosmic cosmic contact characteristics between multilayer heterostructures by experiments, numerical simulation is also used to perform the research work. Based on the discrete element method, Lobo Guerrero and Vallejo [15] established a two-dimensional discrete element model of the sleeper track bed to study the impact of ballast breaking on track settlement and analyze the change of force chain distribution of the granular track bed and the process of ballast breaking under cyclic load. Based on the finite element analysis method, Shaer et al. [3] studied the relationship between the ballast deformation and the track settlement from the overall structure. In [16], based on the Bernoulli-Euler beam theory in the finite element method, the meshless method is used to analyze the deformation of the beam element. Kabo [17] used the finite element method to establish an overall model of the ballast bed and studied the influence of the ballast shoulder form on the lateral resistance of the ballast bed. In [18], based on dynamic theory and finite element method, five different track models are established to study the mechanical properties of the ballasted track under high-frequency load. Gao et al. [19] established the three-dimensional model of the ballast bed and sleeper by the discrete element method and studied the influence of important factors such as ballast slope, thickness, top width, and shoulder height on the cross-section size of the ballast bed.

The ballast bed is of discrete material, but the track structure is of continuous medium. When analyzing the interaction between the ballast bed and track structure, it is impossible to use a single discrete element method or finite element method to analyze the interaction between the track structure and the track structure. Therefore, to address the coupling dynamics, many scholars, e.g., Gao and Xu [20] and Ngo et al. [21], built the numerical model of the granular ballast soil subgrade based on the coupling algorithm of discrete element and finite difference, analyzed the interface stress of its interaction, and verified the correctness of the model through the field measurement results. Dowding and Gilbert [22], Michael et al. [23], and Nishiura et al. [24] established the coupling models of the bulk track bed and track structure by means of the coupling method of discrete element and finite element to study the mechanical characteristics of the ballasted track. The coupling of the discrete element, the finite element, and the finite difference method provides a new method for studying the interaction between the ballast and the track structure. However, these above-mentioned results are still far from the mature one. Specifically, in viewing the current research results, they mainly suffer from the following problems: (1) the numerical model is mostly based on two-dimensional dynamics and some three-dimensional calculation models are all scaled models; (2) the major objective is on the interaction between the ballast bed and the lower subgrade foundation, while only few of them focus on the interaction between the ballast bed and the upper track; and (3) the calculation process does not consider the adjacent sleepers, such that it cannot fully simulate the high-speed moving train load.

In view of the abovementioned deficiencies, this work first utilizes the laser scanning method to form the ballast model, and then based on the discrete and continuum coupling algorithm, we establish the coupling solution model of the ballast bed and upper track structure with three sleepers in the contact layer between the track bed and the track structure, and the contact force of the discrete element and the displacement information of the nodes of the finite element mesh are transmitted continuously. Thus, the mechanical coupling of the multilayer medium structure can be realized. On this basis, the distributed control loading mode is adopted to load the cyclic load with a certain phase difference on the three sleepers to simulate the moving load of the high-speed train. The mechanical characteristics and micromechanism of the ballast bed and continuous track structure under the dynamic load of high-speed train are studied, and the rationality of the model is verified by comparing with the existing research results. The relevant conclusions can provide scientific basis for the design and regulation of the ballasted track, and the model can also provide a reference for the further design of the test model and the design of the corresponding loading control system.

2. The Principle of Discrete-Continuous Medium Coupling Algorithm

In this paper, the coupling simulation model of the track structure and bulk track bed is established to simulate the interaction between the track structure and track structure under the cyclic load of train. In the process of analysis, the key point is the transfer of mechanical parameters between the discrete track bed and the continuous track structure on the coupling contact surface. Figure 1 shows the transfer mode of mechanical parameters in the coupling process.

The basic kinetic equation of particles in the figure is [25]

$$\begin{cases} m^i \ddot{r}^i = \sum_{j=1}^{N_i} F^{ij} + R^i, \quad i = 1, \ldots, N, \\ J^i \ddot{\theta}^i = \sum_{j=1}^{N_i} q^{ij} \times F^{ij} + K_e^i, \quad i = 1, \ldots, N, \end{cases} \tag{1}$$

where m^i is the mass of particles, J_i is the moment of inertia of particles, r^i and θ^i are the center position and angle vector of particles, F^{ij} is the force exerted on particle i by contacting

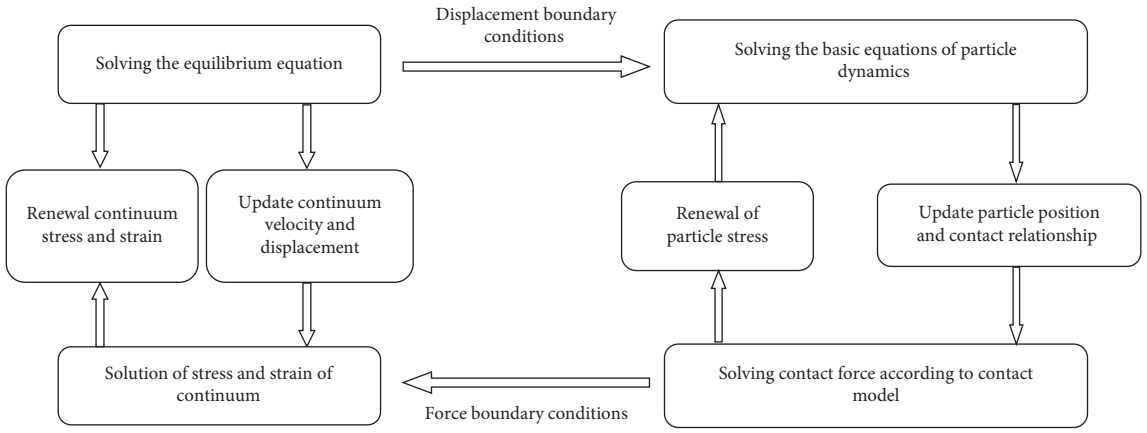

Figure 1: Coupled solution process of discrete-continuous medium.

particle j, q^{ij} is the moment from force F^{ij} to the particle centroid i, R^i and K_e^i are the external forces and moments on particle i, respectively, N_i is the number of particles in contact with i, and N is the total number of particles in the system.

The equilibrium equation of continuum is as follows:

$$M\ddot{u} = -(C\dot{u} + Ku) + F_e, \tag{2}$$

where $\ddot{u}$, $\dot{u}$, and u represent, respectively, acceleration, velocity, and displacement of continuum nodes, M, C, and K are the mass, damping, and stiffness matrices, respectively, and F_e is the node load.

Since the contact force on the coupling surface is usually not located on the nodes of the finite element mesh, the difference method of type row number is used to transfer the contact force from the discrete element domain to the finite element domain. In the finite element analysis of the track mechanism, the 8-node hexahedron isoperimetric element is used to mesh, and the virtual work of the contact force on the contact surface is

$$\delta W = \delta U^T P, \tag{3}$$

where P is the contact force on the coupling contact surface and U is the displacement vector at the contact point, which is obtained by interpolation of node displacement and type function as follows:

$$U = N_i^8 u_i, \quad i = 1 \sim 8, \tag{4}$$

where N_i^8 is the shape function of the 8-node parameter element at the contact point and u_i is the node displacement of element.

The virtual work of the equivalent node force at the node is

$$\delta W_e = \delta u_i F_e, \tag{5}$$

where F_e is the equivalent joint force and $\delta W = \delta W_e$ can be obtained from the principle of virtual work so that the equivalent nodal force is given as follows:

$$F_e = \left[N_i^8\right]^T P, \quad i = 1 \sim 8, \tag{6}$$

with

$$N_i(\xi, \eta, \zeta) = \frac{1}{8}(1 + \xi\xi_i)(1 + \eta\eta_i)(1 + \zeta\zeta_i), \quad i = 1, 2, 3, \ldots, 8, \tag{7}$$

where ξ_i, η_i, and ζ_i are the coordinate values of the node (ξ_i, η_i, ζ_i), $(i = 1, 2, 3, \ldots, 8)$ in the local coordinate system, which can be taken as 1 or −1.

3. Coupling Model of Ballast Bed and Track Structure of High-Speed Railway

3.1. Establishment of Three-Dimensional Model of Fine Ballast Particles. The shape of ballast particles affects the mechanical properties of the particles. The reasonable description of the shape of ballast particles is the key to realize the numerical simulation of the ballast bed. In order to establish a discrete element model that can simulate the real shape of the ballast, a three-dimensional laser scanning platform composed of a computer, a laser scanner, and a rotating platform is built to obtain the real shape of the ballast, as shown in Figure 2. The scanning range of the laser scanner is $200 \times 320 \times 180$ mm, the scanning accuracy is higher than 0.05 mm, and the average point distance is 0.075 mm. Previous studies have shown that when the number of selected typical ballast particles is more than 10, the impact of increasing the number of particle shape samples on the simulation accuracy can be ignored [26]. Therefore, in this paper, 12 kinds of typical ballast particles are selected from a batch of high-speed railway ballast particle samples for fine modeling, and Figure 3 shows one of the typical ballast particle modeling process.

According to Figure 3, the modeling process of ballast particles is as follows. Firstly, the particle surface point cloud image is obtained through the three-dimensional laser scanning platform for ballast particles shown in Figure 2. Then, according to the point cloud of the particle surface obtained by scanning, the closed grid of the particle surface is constructed to realize the reconstruction of ballast geometry. Finally, the geometric profile of ballast particles is filled. At present, there are two forms of three-dimensional ballast particles: spherical cluster particles and bonded particles. The bonding particles can consider ballast

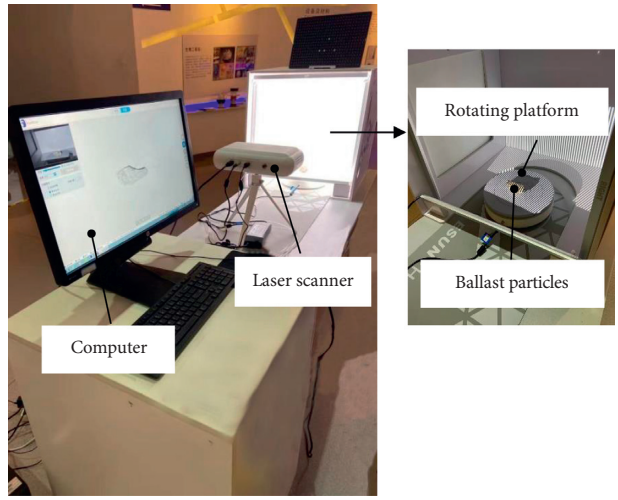

Figure 2: Three-dimensional laser scanning platform for ballast particles.

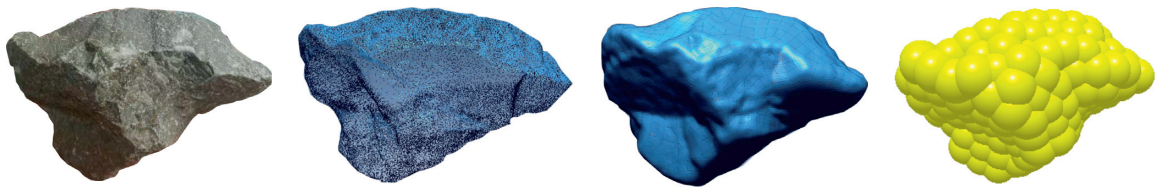

Figure 3: Modeling process of ballast particles: (a) true shape of ballast particles, (b) point cloud image of the ballast particle surface, (c) outer boundary of ballast particles, and (d) model of ballast particle cluster.

crushing, but for the full-scale simulation model, the amount of calculation is too large. Therefore, this paper uses multiball cluster particles to simulate the ballast. When the spherical cluster model is established, the grid coordinate information is obtained by meshing, and the appropriate spherical element radius for filling is selected according to the grid size, and then the ballast particle spherical cluster model is established by API program based on the grid coordinates and spherical element radius. The other 11 kinds of typical ballasts are finely modeled according to the modeling method shown in Figure 3, and the ballast particle geometric profile and ball cluster model are obtained, as shown in Figure 4.

In addition, the model of ballast sphere cluster can be simplified by increasing the mesh size and the radius of sphere element used for filling. It reduces the number of spheres that make up the ballast particles, reduces the number of contact search and judgment of particles in the calculation process, and improves the calculation efficiency. Figure 5 shows the comparison before and after simplification of the ballast particle cluster model.

3.2. Coupling Model of Ballast Bed and Track Structure of High-Speed Railway. The number of spheres in the spherical cluster model in Figure 4 is reduced without affecting the geometric shape of the particles. According to the special ballast particle gradation curve shown in Figure 6, typical shape particles are randomly generated into ball cluster models with different particle sizes, and the coupling model of high-speed railway ballast track and track structure is established, as shown in Figure 7. When the train passes, the area of vertical dynamic wheel load is mainly concentrated in the area covered by three sleepers under the axle, which bears more than 85% of the load [27]. Therefore, in order to simulate the force effect of adjacent sleepers and eliminate the influence of displacement boundary, the simulation analysis model established includes at least three sleepers. The fixed wall boundary is set at the bottom and side of the ballast bed, respectively, while the top surface and slope of the ballast bed are free boundary. In addition, in order to truly represent the shape and corner features of the sleeper, the wall is used to simulate the sleeper.

High-speed railway requires that the ballast should be made of super granite and the sleeper should be type III concrete sleeper. The physical parameters of the ballast and sleeper are shown in Table 1.

Due to the ball cluster model used to simulate ballast particles, there is no sticky spherical surface in ballast particles and the simulated ballast bed is in a state of no dirt. Therefore, the contact between ballast particles and between ballast and geometry is a general contact. Therefore, in this paper, the Hertz–Mindlin (no-slip) contact model is used to simulate the contact between ballast particles, as well as between the ballast and sleeper and boundary. The specific contact parameters are shown in Table 2.

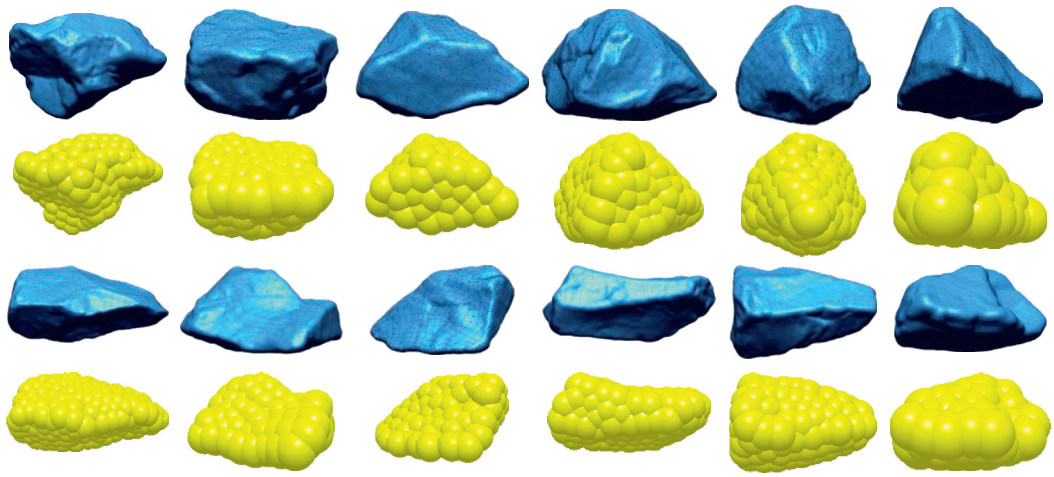

Figure 4: Geometric profile and ball cluster model of typical ballast particles.

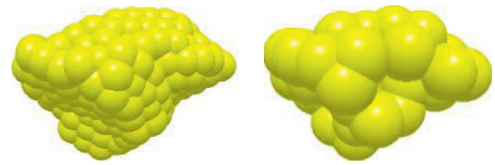

(a) (b)

Figure 5: Comparison of the ballast ball cluster model before and after simplification: (a) particle cluster model and (b) simplified particle cluster model.

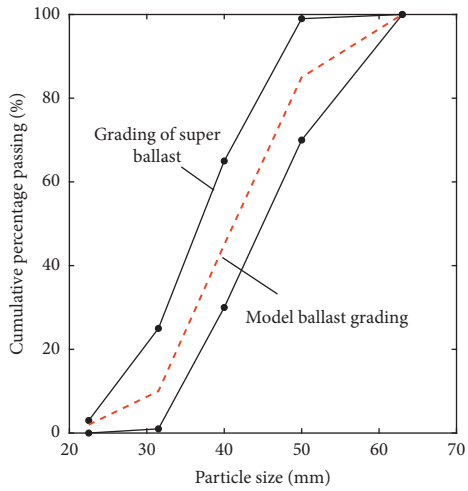

Figure 6: Grading curve of ballast particles.

4. Moving Load Simulation and Control Loading Mode of High-Speed Vehicle with Ballast Bed

In this paper, the CHR2 type high-speed train in China is taken as the research plant, the track irregularity of Qinhuangdao Shenyang passenger dedicated line is taken as the excitation, and the vertical coupling dynamic model of the high-speed train ballasted track described in reference [28] is used to calculate the fulcrum force acting on the rail when the EMU operates at speed of 160 km/h, 200 km/h, 250 km/h, 300 km/h, and 350 km/h, respectively. Through the abovementioned calculation, the rail fulcrum amplitudes corresponding to different speeds are 24.8 kN, 25 kN, 25.4 kN, 26 kN, and 28.8 kN, respectively. Figure 8 is the schematic diagram of the middle car body of the CHR2 high-speed train set. It can be seen from Figure 8 that the distance between the two bogies in the middle car is 17500 mm, and the distance between the bogie and both ends of the car is 3500 mm. In order to accurately simulate the train load, the distance between the two bogies is used as the train load interval. Therefore, the train passing frequencies corresponding to the abovementioned speeds are obtained by equation $f = v/L$, which are 2.54 Hz, 3.17 Hz, 3.97 Hz, 4.76 Hz, and 5.56 Hz. In the formula, f is the passing frequency, v is the driving speed, and L is the distance between the bogies. Given the amplitude of rail fulcrum force and train passing frequency, the curve of train cyclic load can be obtained, considering the load phase difference of adjacent sleepers, and the train cyclic load curve of three sleepers in 1 s under the speed of 250 km/h is shown in Figure 9.

The controlled loading mode of the moving load of the high-speed vehicle is shown in Figure 10. As can be seen from Figure 10, when the vertical wheel load of the train acts directly above the middle sleeper, the loading forces shared by the three sleepers are F_1, F_2, and F_3, respectively. G_1, G_2, and G_3 in the picture represent the weight of the three sleepers, respectively. When the high-speed train passes

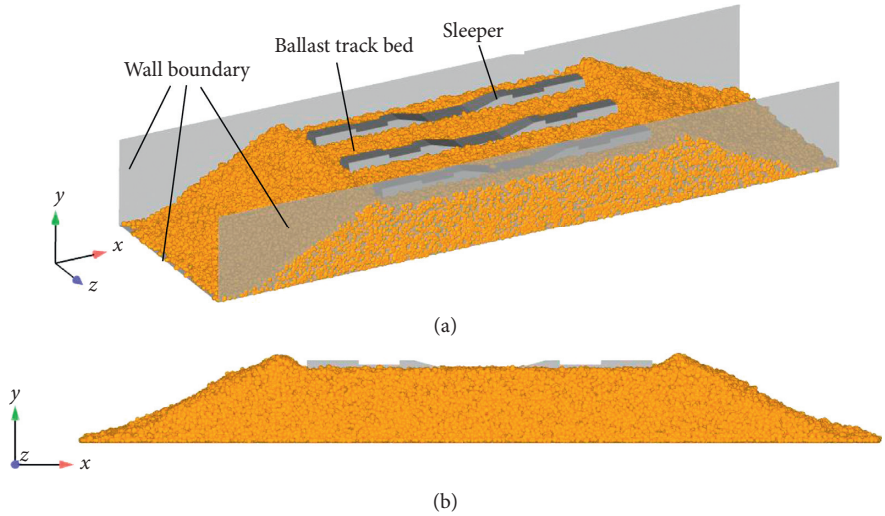

Figure 7: Coupling model of the ballasted bed and track structure of high-speed railway: (a) general view and (b) main view.

Table 1: Physical parameters of the ballast and sleeper.

Physical parameters	Ballast	Type III concrete sleeper
Density (kg·m^{-3})	2700	2000
Poisson's ratio	0.25	0.25
Shear modulus (Pa)	1.0×1010	1.44×1010

Table 2: Contact parameters of the discrete element model.

Contact parameter	Between ballast particles	Between ballast particles and sleeper and side boundary
Restitution coefficient	0.6	0.6
Coefficient of static friction	0.8	0.86
Dynamic friction coefficient	0.1	0.03

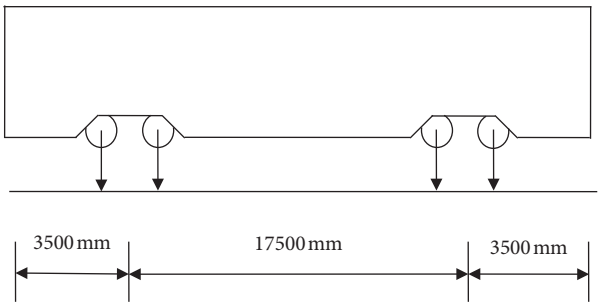

Figure 8: Cyclic load curve of train with speed of 250 km/h.

through the ballast bed, the moving wheel load acting on the sleeper through the rail is the moving load. The distributed control loading mode is adopted to realize the independent control of the loading force, and the phase difference of the loading forces F_1, F_2, and F_3 of the adjacent sleepers is controlled by writing the loading program so that the moving loading of trains with different speeds can be completed. In addition to the moving load transmitted by the sleeper, the ballasted bed also bears the weight of the sleeper, so a servo is introduced to apply gravity to the wall sleeper in the process of calculation.

5. Mechanical Characteristics of Ballasted Bed of High-Speed Railway

5.1. Dynamic Characteristics and Settlement of Loose Ballast Bed

5.1.1. Dynamic Characteristics of Ballast Contact Force under Dynamic Load of High-Speed Train. In order to study the change of ballast contact force in the ballast bed when the high-speed train passes, Figure 11 shows the spatial distribution of ballast contact force vector before the train passes and when the train passes at 200 km/h, 250 km/h, and 300 km/h. Figure 11(a) shows the spatial distribution of the ballast contact force vector in the track bed before the train passes. Figures 11(b)–11(d), respectively, show the spatial distribution of the ballast contact force vector when the train passes at 200 km/h, 250 km/h, and 300 km/h. In the figure, the direction of the solid line segment indicates the contact force direction of the ballast, and the color of the solid line segment indicates the contact force. It can be seen from Figure 11(a) that the contact force of the ballast in the ballast bed is evenly distributed before the train passes through, only a small amount of large contact force appears under the sleeper, and the contact force of the ballast before loading is

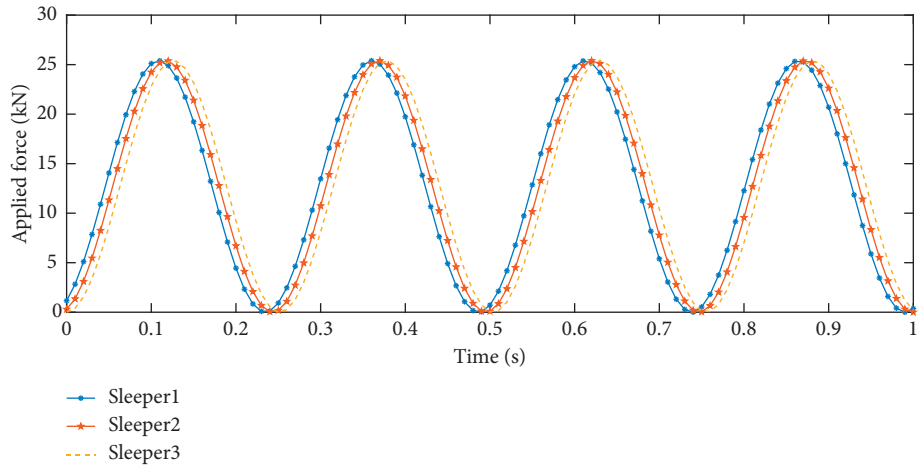

Figure 9: Cyclic load curve of train with speed of 250 km/h.

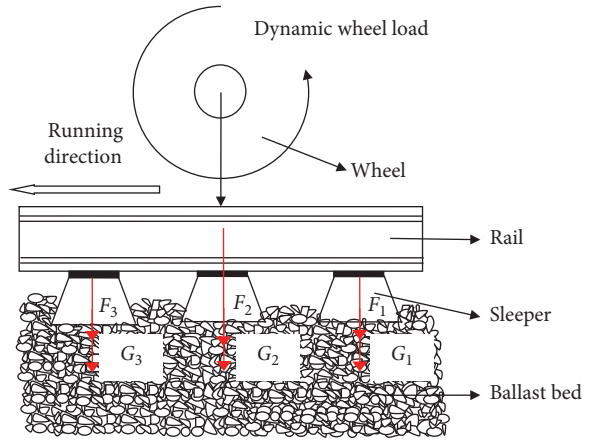

Figure 10: Control loading mode of moving load of high-speed vehicle.

very small because the ballast bed is not compacted before loading. It can be seen from Figures 11(b)–11(d) that the train passes at a certain speed, the ballast contact force inside the ballast bed is not evenly distributed, and the contact force is mainly distributed on the bottom of the sleeper, and the direction is spread in the form of trapezoid downward, which is basically consistent with the previous research [29].The contact around the sleeper is relatively large, but the contact force is mainly distributed in the shallower position directly below the sleeper. With the increase of the depth of the ballast bed, the contact force of the ballast decreases continuously, which shows that the ballast bed can disperse and reduce the train load. The higher the driving speed, the more uneven the spatial distribution of the contact force vector of the ballast in the track bed, and the contact force increases with the increase of speed.

At different speeds, the maximum and average contact force of ballast in the ballast bed is shown in Figure 12. As it can be seen from Figure 12, there is a significant difference between the maximum contact force and the average contact force between ballasts, mainly because the ballast particles of the ballast shoulder are generally at rest when the train passes. The results show that the maximum contact force and average contact force of the ballast increase with the increase of speed. When the driving speed is 160 km/h, the maximum contact force of ballast is 7372.1 N, and the average contact force is 3.13 N. When the driving speed is 250 km/h, the maximum contact force of the ballast is 7425.3 N, and the average contact force is 3.20 N, increasing by 0.72% and 2.2%, respectively. When the driving speed increases to 350 km/h, the maximum contact force of the ballast is 7647.0 N, the average contact force is 10.0 N, the maximum contact force increases by 3.73%, and the average contact force increases by 3.2 times. The abovementioned analysis shows that the higher the driving speed is, the greater the contact force of ballast will be. When the driving speed reaches 250 km/h, the growth rate of contact force will be high rapidly.

5.1.2. The Change of Ballast Angular Velocity under Dynamic Load of High-Speed Train. The rearrangement of ballast particles is the main factor affecting the stability of the ballast bed and also the direct factor causing the settlement of the ballast bed. The rearrangement of ballast particles is mainly due to the contact sliding and rotation between ballast particles, in which the relative rotation angular velocity of ballast particles describes the overall rotation angle of ballast particles. Figure 13 shows the change of ballast rotation angle speed under different driving speeds when the load reaches the peak value. It can be seen from the figure that the greater the train speed, the greater the average speed of the ballast. When the running speed varies from 160 km/h to 300 km/h, the average speed of the ballast changes slowly. When the speed is 350 km/h, the ballast speed increases significantly. From the figure, due to the discreteness of the ballast bed, the maximum velocity of ballast particles has no obvious rule.

5.1.3. Effect of Driving Speed on Cumulative Settlement of Ballast Bed. The ballast will produce movement and deformation during the train load cycle, which will lead to the settlement of the ballast bed. The uneven settlement of track

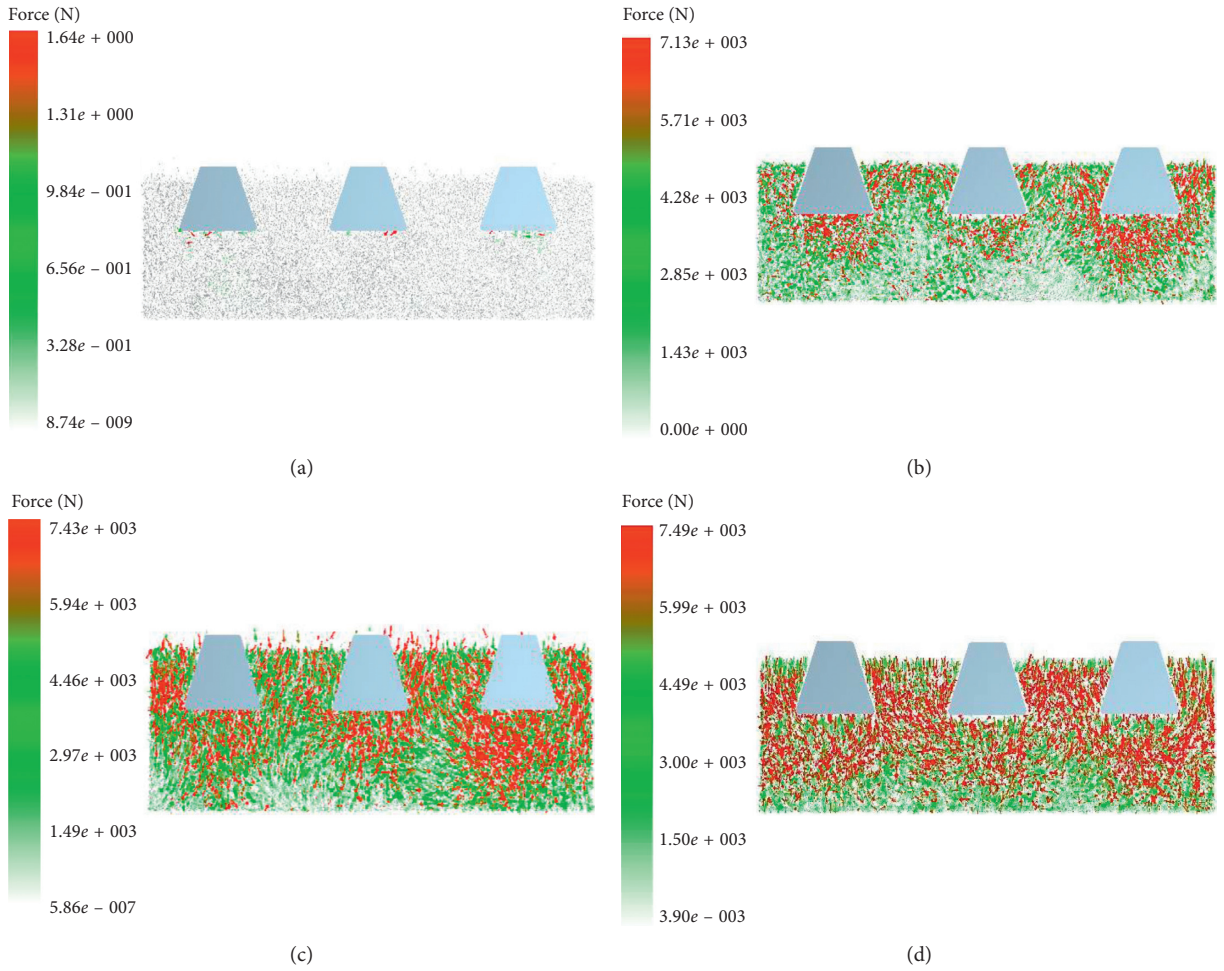

Figure 11: Spatial distribution of ballast contact force: (a) before train passing, (b) when the train passes at 200 km/h, (c) when the train passes at 250 km/h, and (d) when the train passes at 300 km/h.

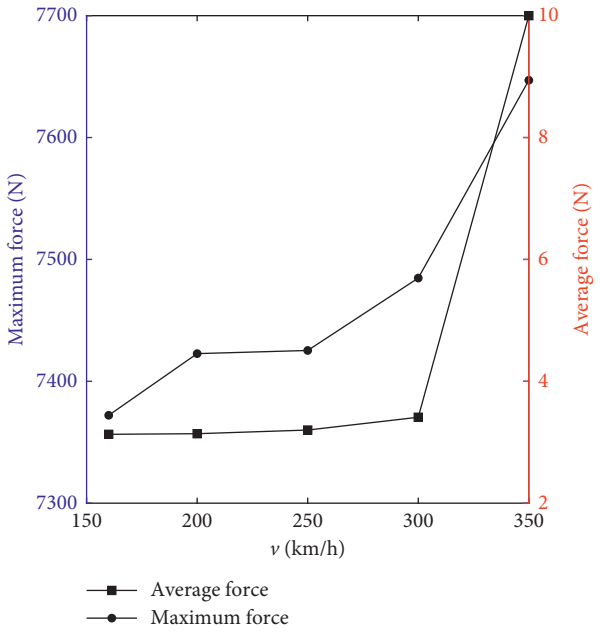

Figure 12: Maximum and average contact force of the ballast at different speeds.

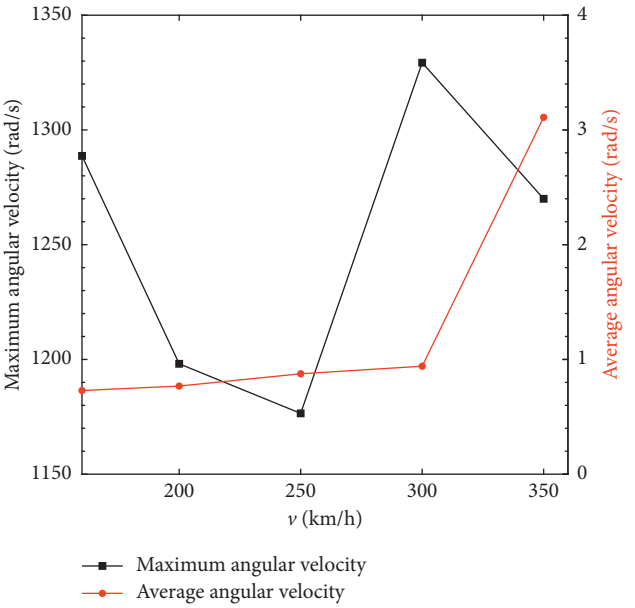

Figure 13: Maximum and average value of ballast angular speed at different speeds.

bed leads to track irregularity, which directly threatens the safety of train operation. The running speed of high-speed train is one of the main factors affecting the stability of the ballasted track so that it is necessary to study the settlement characteristics of ther ballast bed from the aspect of train running speed. In the coupling model established in this paper, the wall is used to simulate the sleeper and endow the sleeper with weight so that the sleeper is in the direct contact with the ballast, and the settlement of the track bed can be expressed by the vertical settlement of the sleeper. In order to ensure the reliability of the results, the settlement of the middle sleeper in the vertical direction is selected to represent the ballast settlement, and the relationship between driving speed and ballast cumulative settlement is obtained, as shown in Figure 14. It can be seen from Figure 14 that the larger the driving speed is, the faster the accumulated settlement and settlement speed of the ballast bed will be. As the ballast bed is not compacted in the layers, the settlement of the ballast bed is large at the initial stage of loading. With the increase of loading times, the settlement speed of the ballast bed becomes slow.

To sum up, the running speed of high-speed trains directly affects the force chain distribution, the contact force size, and the relative rotation speed of ballast particles in the ballast bed, and the greater the running speed, the greater the contact force and rotation speed between the ballast. However, the mutual movement of ballast particles leads to the settlement of the ballast bed so that the larger the driving speed is, the greater the accumulated deposition speed and the accumulated settlement of ballast bed are.

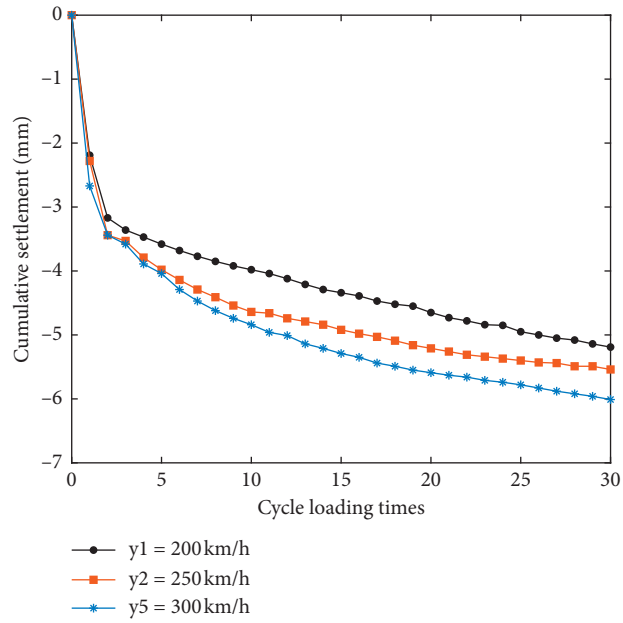

Figure 14: Driving speed and ballast bed settlement.

5.2. The Force Acting on the Track Structure and the Settlement Characteristics of the Track Bed

5.2.1. Analysis of Contact Characteristics between Sleeper and Ballast. When the high-speed train is running, there will be interaction between the sleeper and ballast under the action of train load. The coupling model of the ballast bed and track structure was established to analyze the contact between the sleeper and ballast at different running speeds.

Figure 15 shows the contact between the ballast and the sleeper when the load reaches the peak. In Figure 15, the direction of the solid line segment indicates the direction of contact force, and the color and thickness of the solid line segment indicate the contact size. As it can be seen from the figure, the number of contacts between the ballast and the end face of the sleeper is the least, and the contact force is also relatively small. Although there are many contacts on the side of sleeper, the contribution to the resistance of the ballast bed is relatively small. The contact force between the sleeper and ballast bed mainly comes from the bottom of the sleeper, which is consistent with previous research results [7].

Figure 16 shows the relationship between the number of contacts and between the ballast and sleeper when the driving speed is 250 km/h. It can be seen from the figure that when the train passes, the ballast particles in the track bed will rotate, slide, and rearrange continuously, which will lead to the continuous fluctuation of the number of contacts between the ballast and the sleeper. The number of contacts between the middle sleeper and the ballast is relatively low, indicating that the resistance of the middle sleeper is less than that of the other two sleepers. It shows that the wall boundary has a significant influence on the sleeper, and the scale model considering only one sleeper has limitations in the process of calculation.

Figure 17 shows the relationship between the number of contacts and between the ballast and intermediate sleeper with time at different driving speeds. As it can be seen from the figure, due to the lack of layered compaction of the ballast, the number of contacts between the sleeper and the ballast increases rapidly at the beginning of loading. When the driving speed is 160 km/h, 200 km/h, 250 km/h, and 300 km/h, the contact number between the sleeper and ballast is similar, and the change trend of the contact number with time is stable. When the driving speed is 350 km/h, the number of contacts between the sleeper and ballast is relatively large, and the number of contacts changes greatly. Due to the discrete characteristics of ballast bed, the number of contacts between the ballast and sleeper has no obvious rule under different driving speeds, and it proves the discreteness of contact between the sleeper and ballast bed.

5.2.2. Analysis of Contact Strength between Sleeper and Ballast Bed. The contact strength between the sleeper and ballast bed is the ratio of contact force and contact area between the bottom of the sleeper and ballast bed, where the contact area is 7228.56 cm^2. Since the contact area is constant, the change trend of contact force and contact strength is consistent. Figure 18 shows the contact strength between the bottom of the sleeper and the ballast at different driving speeds. It can be seen from the figure that the change trend of contact strength is close to the change trend of contact force and rotation speed of ballast particles in Figures 7 and 13.

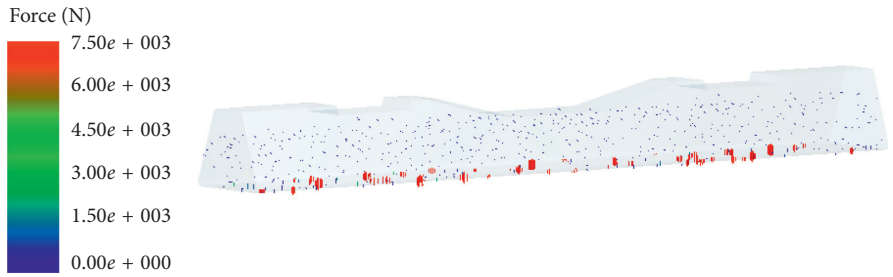

Figure 15: Contact distribution between the ballast and sleeper.

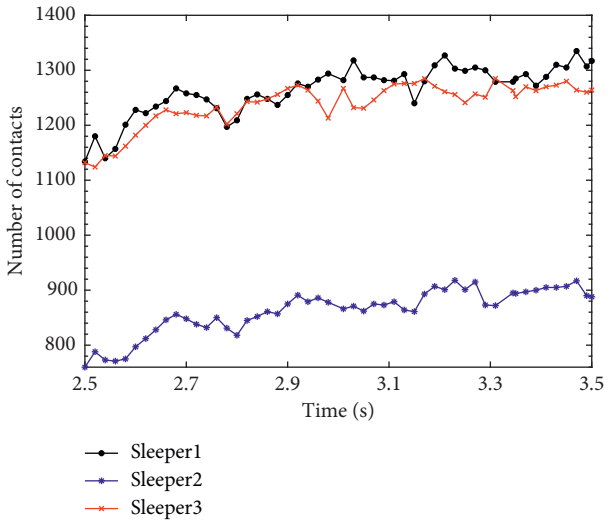

Figure 16: Number of contacts between the ballast and sleeper.

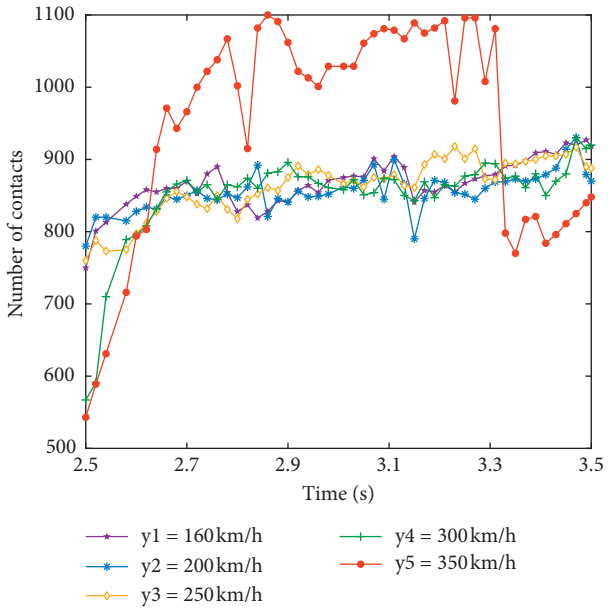

Figure 17: The relationship between the number of contacts between the ballast and sleeper with time.

And with the increase of driving speed, the value of contact strength increases, which means that the contact force increases with the increase of driving speed. Compared with

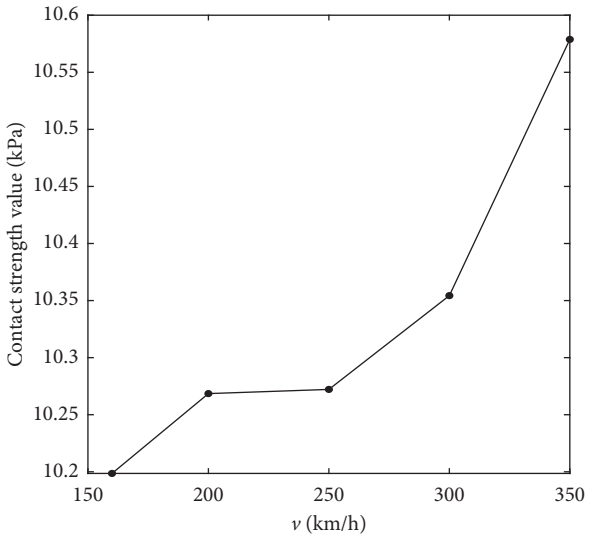

Figure 18: Contact strength between the sleeper and ballast.

Figure 14, the greater the contact strength between the sleeper and the ballast is, the faster the settlement speed of the ballast bed is and the greater the settlement is.

6. Conclusion

(1) In this paper, the three-dimensional laser scanning method is used to establish the real model of the ballast, and then the coupling model of the ballast bed and upper track structure with three sleepers is established based on the coupling method of the discrete body and continuous body. The analysis of the contact between three sleepers and ballast shows that the wall boundary has a significant impact on the sleepers, and the coupling model considering only one sleeper has limitations in the calculation process. The conclusion can provide a reference for further research on the coupling modeling of the ballast bed and track structure.

(2) Based on the coupling model of the ballast bed and track structure, the macro- and microdynamic characteristics of the ballast bed under the dynamic load of high-speed trains with different speeds are studied. The results show that the running speed of the high-speed train directly affects the force chain

distribution of the ballast in the ballast bed, the contact force between ballast particles and the relative rotation speed of ballast particles. The larger the driving speed is, the larger the contact force and rotation speed between the ballasts will be, which will eventually lead to the increase of the accumulated deposition speed and the accumulated settlement amount of the ballast bed with the increase of the driving speed. This conclusion provides a reference for the study of macroscopic and mesoscopic characteristics of the ballast bed settlement.

(3) The coupling contact between the ballast bed and track structure is studied. The results show that the ballast has contact with the end, side, and bottom of the sleeper. Although there are a large number of contacts between the ballast and the side of the sleeper, the contact force here is relatively small, and the contact force between the sleeper and the ballast bed mainly comes from the bottom of the sleeper. In addition, the contact strength and contact force between the sleeper and the track bed are directly proportional to the driving speed. The conclusion provides a reference for the study of the coupling contact between the ballast bed and the track structure.

(4) The distributed control method is used to simulate the moving load of the high-speed train. The research results provide reference for the further design of the test model and the design of the corresponding loading control system.

Data Availability

The data used to support the findings of this study are available from the corresponding author upon request.

Conflicts of Interest

The authors declare that they have no conflicts of interest.

Acknowledgments

This work was supported by the Natural Science Foundation of China (NSFC) under Grant nos. 51565021 and 51965029.

References

[1] Y. Guo, V. Markine, X. Zhang, W. Qiang, and G. Jing, "Image analysis for morphology, rheology and degradation study of railway ballast: a review," *Transportation Geotechnics*, vol. 18, pp. 173–211, 2019.

[2] A. M. Kaynia, C. Madshus, and P. Zackrisson, "Ground vibration from high-speed trains: prediction and countermeasure," *Journal of Geotechnical and Geoenvironmental Engineering*, vol. 126, no. 6, pp. 531–537, 2000.

[3] A. A. Shaer, D. Duhamel, K. Sab, G. Foret, and L. Schmitt, "Experimental settlement and dynamic behavior of a portion of ballasted railway track under high speed trains," *Journal of Sound & Vibration*, vol. 316, no. 1–5, pp. 211–233, 2008.

[4] T. Ishikawa, E. Sekine, and S. Miura, "Cyclic deformation of granular material subjected to moving-wheel loads," *Canadian Geotechnical Journal*, vol. 48, no. 5, pp. 691–703, 2011.

[5] Y. Koike, T. Nakamura, K. Hayano, and Y. Momoya, "Numerical method for evaluating the lateral resistance of sleepers in ballasted tracks," *Soils and Foundations*, vol. 54, no. 3, pp. 502–514, 2014.

[6] J. Kennedy, *A full-scale laboratory investigation into railway track substructure performance and ballast reinforcement*, Ph.D. dissertation, Heriot-Watt University, Edinburgh, UK, 2011.

[7] G. Q. Jing, H. Fu, W. L. Jia et al., "Macro-micro analysis of lateral resistance for high speed railway ballasted track," *Journal of Railway Engineering Society*, vol. 35, no. 9, pp. 24–28, 2018, in Chinese.

[8] H. Faghihi Kashani, J. P. Hyslip, and C. L. Ho, "Laboratory evaluation of railroad ballast behavior under heavy axle load and high traffic conditions," *Transportation Geotechnics*, vol. 11, pp. 69–81, 2017.

[9] Y. Momoya, T. Takahashi, and T. Nakamura, "A study on the deformation characteristics of ballasted track at structural transition zone by multi-actuator moving loading test apparatus," *Transportation Geotechnics*, vol. 6, pp. 123–134, 2016.

[10] Z. Yu, D. P. Connolly, P. K. Woodward, and O. Laghrouche, "Settlement behaviour of hybrid asphalt-ballast railway tracks," *Construction and Building Materials*, vol. 208, pp. 808–817, 2019.

[11] Q. M. Zhu, D. Y. Zhao, and J. H. Zhang, "A general U-block model based design procedure for nonlinear polynomial control systems," *International Journal of Systems Science*, vol. 47, no. 17, pp. 3465–3475, 2016.

[12] Q. Zhu, W. Zhang, J. Zhang, and B. Sun, "U-neural network-enhanced control of nonlinear dynamic systems," *Neurocomputing*, vol. 352, pp. 12–21, 2019.

[13] Q. Zhu, L. Liu, W. Zhang, and S. Li, "Control of complex nonlinear dynamic rational systems," *Complexity*, vol. 2018, Article ID 8953035, 12 pages, 2018.

[14] X. Geng, Q. Zhu, T. Liu, and J. Na, "U-model based predictive control for nonlinear processes with input delay," *Journal of Process Control*, vol. 75, pp. 156–170, 2019.

[15] S. Lobo-Guerrero and L. E. Vallejo, "Discrete element method analysis of railtrack ballast degradation during cyclic loading," *Granular Matter*, vol. 8, no. 3-4, pp. 195–204, 2006.

[16] Y. Tian, C. Zhang, and Y. Z. Sun, "The application of meshfree method in the numerical simulation of beams with the size effect," *Mathematical Problems in Engineering*, vol. 2014, Article ID 590271, 6 pages, 2014.

[17] E. Kabo, "A numerical study of the lateral ballast resistance in railway tracks," *Proceedings of the Institution of Mechanical Engineers, Part F: Journal of Rail and Rapid Transit*, vol. 220, no. 4, pp. 425–433, 2006.

[18] J. Y. Shih, D. Kostovasilis, Y. Bezin et al., "Modelling options for ballast track dynamics," in *Proceedings of the 24th International Congress on Sound and Vibration*, London, UK, July 2017.

[19] L. Gao, Q. Luo, Y. Xu et al., "Effects of ballast bed section dimension on its lateral resistance," *Journal of Southwest Jiaotong University*, vol. 49, no. 6, pp. 954–960, 2014.

[20] L. Gao and Y. Xu, "Application of coupled discrete element-finite difference method in railway ballast bed research," *Journal of Beijing Jiaotong University*, vol. 40, no. 4, pp. 37–44, 2016, in Chinese.

[21] N. T. Ngo, B. Indraratna, and C. Rujikiatkamjorn, "Simulation ballasted track behavior: numerical treatment and field application," *International Journal of Geomechanics*, vol. 17, no. 6, pp. 04016130-1–04016130-12, 2017.

[22] C. H. Dowding and C. Gilbert, "Dynamic stability of rock slopes and high frequency traveling waves," *Journal of Geotechnical Engineering*, vol. 114, no. 10, pp. 1069–1088, 2016.

[23] M. Michael, F. Vogel, and B. Peters, "DEM-FEM coupling simulations of the interactions between a tire tread and granular terrain," *Computer Methods in Applied Mechanics and Engineering*, vol. 289, pp. 227–248, 2015.

[24] D. Nishiura, H. Sakai, A. Aikawa, S. Tsuzuki, and H. Sakaguchi, "Novel discrete element modeling coupled with finite element method for investigating ballasted railway track dynamics," *Computers and Geotechnics*, vol. 96, pp. 40–54, 2018.

[25] Z. P. Tang, "Three-dimensional DEM theory and its application to impact mechanics," *Science in China (Series E)*, vol. 44, no. 6, pp. 561–571, 2001.

[26] H. Huang, *Discrete element modeling of railroad ballast using imaging based aggregate morphology characterization*, Ph.D. dissertation, University of Illinois, Urbana, IL, USA, 2010.

[27] V. A. Profillidis, *Railway Engineering*, Ashgate Publishing Linmited, Aldershot, UK, 2000.

[28] X. Zhang, *Numerical Simulation and Experiment Study on Macro-Micro Mechanical Behaviors of High-Speed Railway Ballast*, Southwest Jiaotong University, Chengdu, China, 2017, in Chinese.

[29] D. R. Ahlbeck, H. C. Meacham, and R. H. Prause, "The development of analytical models for railroad track dynamics," in *Proceedings of the Symposium on Railroad Track Mechanics & Technology*, pp. 239–263, Princeton, NJ, USA, January 1978.